SAE International

2013-01-0462
Published 04/08/2013

doi:10.4271/2013-01-0462
saepcmech.saejournals.org

Aerodynamic Drag Reduction on a Simple Car-Like Shape with Rear Upper Body Taper

Jeff Howell
Tata Motors European Technical Centre

Martin Passmore and Simon Tuplin
Loughborough University

ABSTRACT

Various techniques to reduce the aerodynamic drag of bluff bodies through the mechanism of base pressure recovery have been investigated. These include, for example, boat-tailing, base cavities and base bleed. In this study a simple body representing a car shape is modified to include tapering of the rear upper body on both roof and sides. The effects of taper angle and taper length on drag and lift characteristics are investigated. It is shown that a significant drag reduction can be obtained with moderate taper angles. An unexpected feature is a drag rise at a particular taper length. Pressure data obtained on the rear surfaces and some wake flow visualisation using PIV are presented.

CITATION: Howell, J., Passmore, M. and Tuplin, S., "Aerodynamic Drag Reduction on a Simple Car-Like Shape with Rear Upper Body Taper," *SAE Int. J. Passeng. Cars - Mech. Syst.* 6(1):2013, doi:10.4271/2013-01-0462.

INTRODUCTION

Aerodynamic drag of a typical passenger car arises from a near equal split between the styled upper surfaces and the remaining less visual components comprising; cooling airflow, underbody, wheels and wheelarches. On the upper surfaces the major drag component occurs at the rear of the car, Howell, [1], and as this can exceed half the drag of the styled surfaces, dominates the front end drag, skin friction and protuberences such as mirrors. This can constitute over 25% of the overall aerodynamic drag and it results from the suction which occurs on the rearward facing surfaces, especially those in the separated flow regions at the base of the car. Similarly, from the 'unstyled' components, the wheels and wheelarches contribute up to one third of the overall aerodynamic drag, Pfadenhauer et al., [2], while the contribution from the underfloor is in the range of 10-15% approximately. While overall drag reduction is achieved by accumulating many small incremental benefits from all surfaces and components on the car, any major future impact on aerodynamic drag reduction will come from investigating these significant contributors.

Improving the rear end drag must primarily concentrate on increasing the pressure on the base and comes under the general heading of 'base pressure recovery'. The main routes for achieving this are rear body tapering (boat-tailing), base cavities, and base flow injection. A significant amount of research has been conducted on the effect of the base region on drag reduction for axisymmetric bodies at high Mach numbers relevant to missile aerodynamics, as reviewed comprehensively by Viswanath, [3], but only a few studies have been at the low subsonic Mach numbers relevant for automobiles. Drag reduction from base cavities was recently investigated by Howell et al., [4], using a modified Ahmed body. This followed the early study by Morel, [5], with a small scale axisymmetric body and showed that ventilating the cavity allowed the cavity depth to be reduced. Very few experiments on base flow injection, applicable to road vehicle type bodies, have been reported. Exceptions are the work of Englar, [6], with high velocity Coanda type jets, and Sykes, [7] and Howell et al., [8] using low velocity bleed flow. Interestingly, the latter study showed that a significant part of the drag reduction achieved came from the cavity.

The significant potential for drag reduction from boat-tailing of simple elongated bodies in freestream has been investigated by Mair, [9], for axisymmetric bodies and Wong and Mair, [10], for a body of square cross section. Simple rectangular bodies in ground proximity with truncated tapered rear bodies representing truck and bus shapes have been studied by Gilhaus, [11], and Götz, [12], respectively. Significant drag reduction has been demonstrated on trucks with the use of angled base boards to provide a combination of cavity with boat-tailing effects, as exemplified by Cooper,

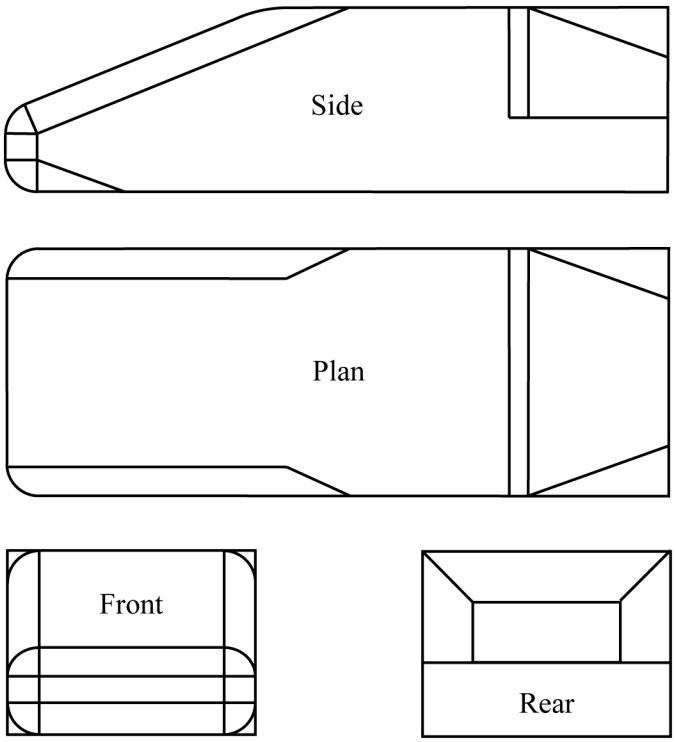

Figure 1. Windsor Body with Upper Rear Body Tapering.

[13], and Browand et al., [14]. Boat-tailing effects can be seen in saloon and fastback car shapes, although the top surface tapering for these vehicles tends to be excessive. It has also been exploited on 1- and 2-box shapes through the combined effects of roof and bodyside curvature, although design and packaging constraints have limited these benefits. In this paper the effects of tapering, (boat-tailing), the upper rear body of a simple car-like shape are investigated.

EXPERIMENTAL STUDY

Model

The simple bluff Windsor Body model used in these tests is shown in Figure 1. The model details have been well documented previously; see for example Howell and Le Good, [15]. The model is 1.044m long, 0.39m wide and 0.29m high, and the overall dimensions represent an approximately quarter scale small hatchback car. The model has a removeable upper rear body section which allows shape variation in this region. For the study reported here the interchangeable body sections were tapered on the roof and upper body sides. The length, L, and angle, ϕ, of the taper were varied, but for any given section, the taper angles were the same on both top and sides. The ground clearance was set at 0.040 m. The model was mounted to an underfloor 6-component balance via four thin supports of 0.008m diameter, which protruded the wind tunnel floor. No adjustment was made for the strut tare drag. The distance between the legs was 0.668 m, symmetrically placed, which represents the 'wheelbase'. Force coefficients are based on frontal area, while moment coefficients are based on frontal area and the 'wheelbase'. The moment centre is located at mid wheelbase on the ground surface.

The taper lengths investigated were 0.075, 0.125, 0.175 and 0.225m, and the taper angles varied from 5° to 25° in 5° steps. The maximum depth of the upper rear body tapered section was 161mm, representing 56% of the overall depth of the body. The longest taper length, L=0.225m, allowed comparison with previous experiments where only the roof taper (backlight) angle was varied and the roof slope length was 0.220m. The initial tests were conducted with a sharp intersection between the tapered rear surfaces and the bodyside and roof, and these were followed by introducing a radiused intersection, except for the 5° tapered rear ends. Some additional rear sections were made, where only the roof was tapered, with a taper angle of 15° and the taper length was varied approximately as above. The data is compared with a baseline configuration; the squareback model with no roof or bodyside taper.

Wind Tunnel

The aerodynamic data for the Windsor model were obtained using the Loughborough University low speed wind tunnel. This wind tunnel is a closed jet facility with a working section 1.9m wide by 1.3m high; (Area 2.5 m^2). The wind tunnel is described by Johl et al., [16]. It has a maximum airspeed of 45m/s and the turbulence intensity at the model location is 0.2%. The data was obtained at a nominal airspeed of 40m/s, which gives a Reynolds No. of 2.8×10^6 based on

model length. The boundary layer displacement thickness is approximately 0.007m at the centre of the balance, with no model present. Blockage corrections, using the standard MIRA continuity-based correction procedure, as detailed in [17], have been applied to the force, moment and pressure coefficients.

Pressure measurements were taken on the tapered rear surfaces and on the vertical base for the body with a 15° taper angle and taper lengths of 0.125 and 0.225m. For comparison, pressure data was obtained for the basic body with a 15° roof slant (backlight) and no bodyside taper, on the roof slant and vertical base, and base pressure data was also taken on the squareback model. The pressure data is corrected for blockage using the standard MIRA correction procedure. PIV measurements were obtained in a transverse frame immediately aft of the model base for a limited range of configurations.

Figure 2. Tapered Windsor Body in the Loughborough University Wind Tunnel

RESULTS

The initial tests were conducted with a limited range of taper angles from 15° to 25°. This was because the data from trucks, [13, 14], suggested the optimum angle was approximately 16° and simple body tests, [9, 10], gave an optimum taper angle of 20°−22°. The data subsequently showed that this range did not capture an optimum taper angle and additional rear body sections were made with a taper angle of 10°, followed considerably later by a further set with a 5° taper angle; both with a range of taper lengths as in the initial experiment. The effect of taper length on the reduction in drag coefficient is shown in Figure 3 for the range of taper angles.

The data is plotted in Figure 3 as a change from the reference squareback configuration. For the squareback configuration the basic aerodynamic coefficients for drag and lift are: C_D = 0.290, C_{LF} = −0.087 and C_{LR} = 0.038. The open symbols with dotted lines represent the rear bodies with a sharp intersection at the leading edge of the tapered surfaces, while the solid symbols and lines represent bodies with this intersection rounded. For the 5° taper case only the sharp edged intersection was tested. Figure 3(a) shows the extremely high drag coefficient that can be obtained for the 25° taper case at certain taper lengths, while Figure 3(b) shows the drag benefits from the smaller taper angles. For these bodies the radiused and sharp intersections give very similar results. An unexpected result for the trend in drag reduction was the local peak which occurred at a model taper length of 125 mm for all taper angles. The limited published data for the effect of roof taper length on car shapes, Buchheim et al., [18], and the effect of base board length on trucks, [13], has not identified this feature although in the case of the truck data the range of taper lengths was considerably shorter than the range tested here.

The effect of taper length and angle on the lift coefficient is shown in Figure 4. Data is presented as incremental to the squareback configuration. In general, lift increases with taper angle. For taper angles 10° to 20°, lift increases to a steady value for taper lengths greater than 125mm. This approximately coincides with the taper length for the local drag peak. For the 25° taper case the maximum lift occurs at the same taper length as the drag peak, 125mm, and then falls. The intersection condition at the taper leading edge, radiused or sharp, has only a small effect on the lift coefficient in all cases except the largest taper angle.

Almost all the lift is generated at the rear axle. The front axle lift is always negative, while the rear axle lift is always positive for this model and the range of configurations tested. The total variation of front axle lift coefficients is in the range C_{LF} = −0.05 to −0.11, while the rear axle lift coefficients vary from C_{LR} = 0.03 to 0.50. Relative to the squareback configuration the front axle lift initially reduces with the shortest taper length of 0.075m and then increases with increasing taper length.

The general trend is for front lift to increase with taper angle. Rear axle lift follows the trend of total lift and in general increases with taper length and angle. The influence of taper on the drag and lift characteristics at yaw are not particularly marked. The drag rise with yaw reduces as taper length increases but the lift curve is similar for all taper lengths.

The lateral aerodynamic characteristics are influenced by taper. Side force and rolling moment at yaw reduce with taper length, and also reduces with taper angle, while yawing moment at yaw increases with increasing taper length and taper angle. The result is summarised in Figure 5 which shows the lateral aerodynamic data obtained at 15° yaw angle. The data is presented as the increase from that obtained on the squareback model and the yaw data is the mean of the measurements at ± 15° yaw angles.

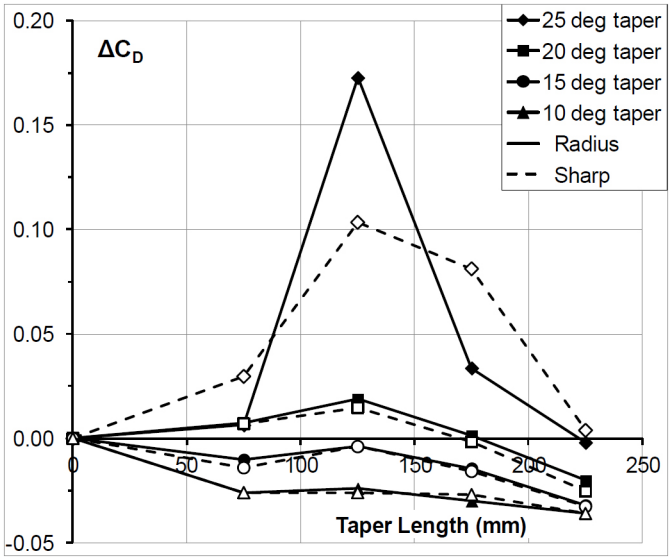

Figure 3(a). Effect of taper length and angle on the drag coefficient.

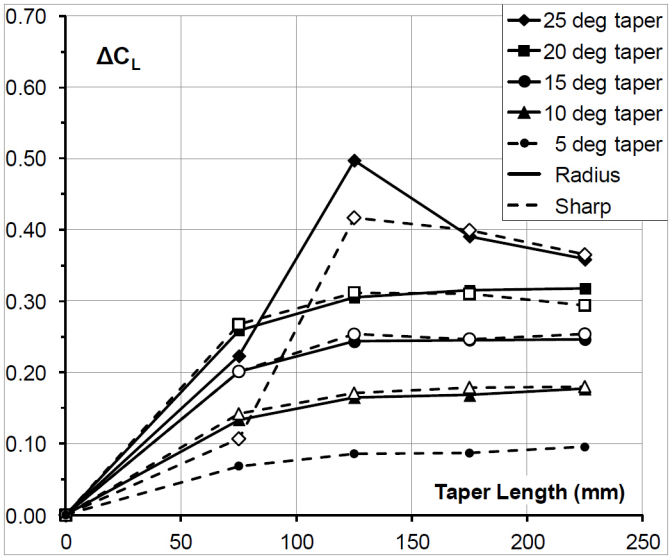

Figure 4. Effect of taper length and angle on the lift coefficient.

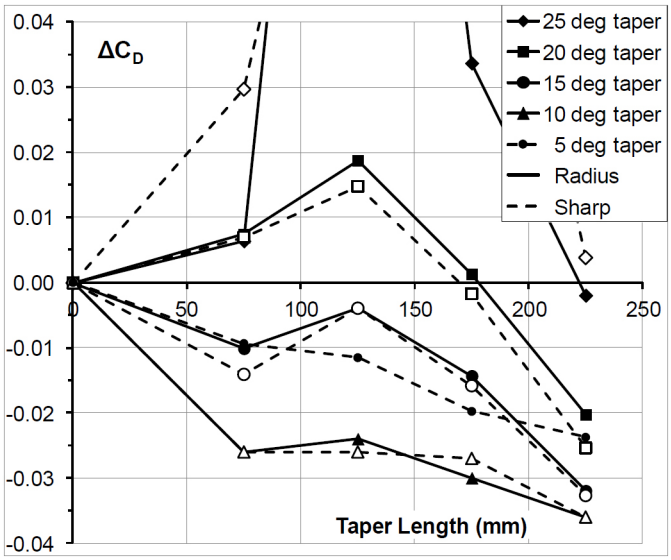

Figure 3(b). Effect of taper length and angle on the drag coefficient-detail.

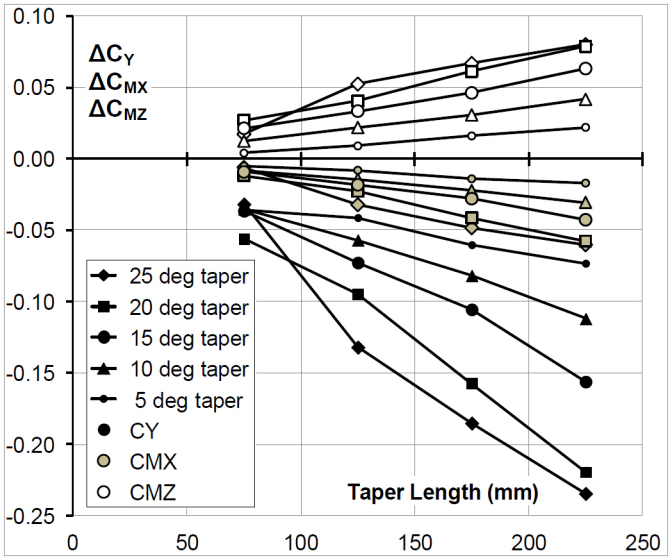

Figure 5. Effect of taper length and angle on the lateral aerodynamic characteristics.

From comparison of the side force and yawing moment trends, it can be deduced that the increase in yawing moment results from a reduction in the side force on the rear body. The drag increase with yaw as obtained at a 15° yaw angle reduces with taper length and with taper angle when compared with the squareback model.

DISCUSSION

An interesting anomaly was found in the drag variation with taper length. As taper length increases it can be seen in Figure 3(b) that for taper angles of 10° and 15°, the drag coefficient initially reduces, as expected, but for taper lengths between 75 and 125mm (model scale) the drag trend reverses and a local drag peak is experienced at taper length of approximately 125mm. For taper lengths greater than 125mm the drag, again, reduces with taper length. This trend is evident for taper angles greater than 10°. At this taper angle the drag reversal has the appearance of a step in the drag trend. It was not clear if this trend was a unique feature of the

rear end geometry adopted in this experiment. From the limited data in the public domain for shapes with no side taper the drag was expected to reduce continuously with roof taper length, changing in magnitude with roof slope; see Buchheim et al., [18].

As a result of this uncertainty, an additional experiment was undertaken to explore the effect of roof taper length on the drag and lift obtained on the Windsor body. The experiment was conducted with a fixed roof taper angle of 15° and the taper length was varied over a similar range to that in the main experiment. This data was supplemented with earlier measurements on the same model by Howell and Le Good, [15], investigating the effects of variable backlight aspect ratio and Littlewood and Passmore, [17], exploring the effect of a small roof trailing edge chamfer. The latter study was carried out using the Loughborough University wind tunnel, while the former investigation was done using the MIRA Model Wind Tunnel (MWT). To limit the effects of any differences arisng from the wind tunnel types or in the set up of the model the drag and lift data is presented in Figure 6 as increments from the values obtained for the squareback model.

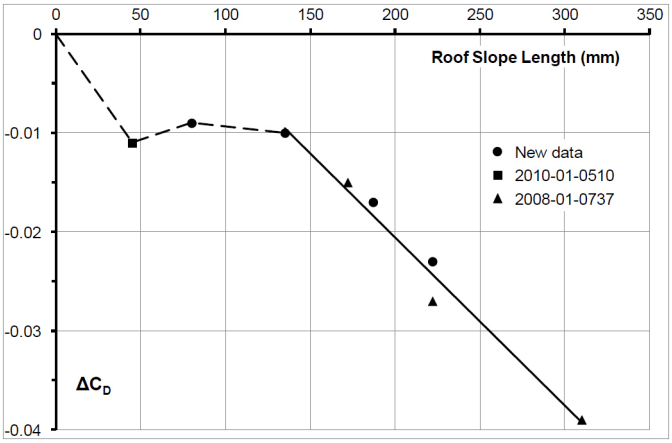

Figure 6(a). Effect of roof slope length on drag coefficient. Roof angle 15°.

The variation in the drag coefficient with roof slope length is shown in Figure 6(a). The data is presented in terms of slope length, where slope length = L/cosφ and L is the taper length and φ is the taper angle. At longer lengths of the sloping roof, where L is greater than 150mm, drag reduces almost linearly. For shorter roof tapers, a change in the drag trend, similar to that shown in Figure 3 is apparent, although care should be taken in interpreting this collated data. It suggests, however, that the drag feature is not confined to the particular geometry used in this study but has more general application. Any discrepancy in this result with that inferred from [18] could be explained by features and components, typical of car shapes, which are not present in the simple bodies tested here.

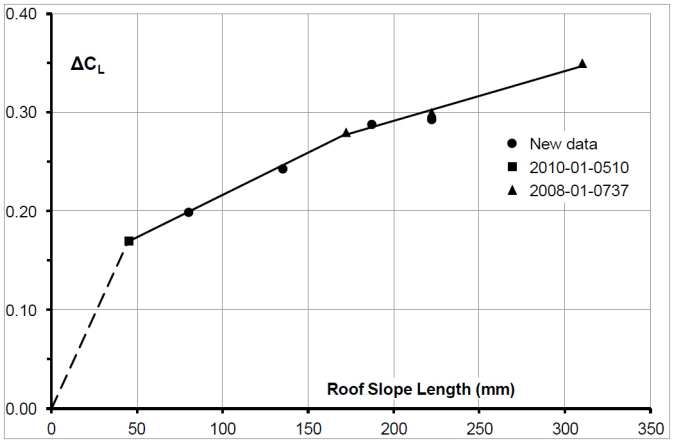

Figure 6(b). Effect of roof slope length on lift coefficient. Roof angle 15°.

The lift coefficient variation with roof slope length is shown in Figure 6(b). For all the configurations tested, lift increases almost linearly with roof slope length. It can be surmised that there is a lift component which arises from the acceleration of the flow over the roof to backlight junction. This grows over a relatively short taper length and then remains constant. To this is added a lift component arising from the vortex which develops on the sharp edges at the sides of the sloping surface.

A plausible explanation for the drag trend of the tapered bodies has been proposed by Han, [19]. Consider Figure 7, which shows, schematically, the drag breakdown and overall lift for a simple body with a tapered rear end of length, L. The values are only indicative. The lift initially increases linearly with taper length and then becomes constant, reflecting the lift variation in Figure 4. The drag is broken down into components representing the forebody drag, C_{DF}, the base drag, C_{DB}, and the drag from the tapered surfaces, C_{DV}. The forebody drag remains essentially constant for all rear end configurations. The base drag will reduce approximately linearly with base area, as shown in [15] and supported by the base pressure measurements given in Table 1. The tapered surfaces generate the lift and these give rise to a drag component, which is predominantly the vortex drag resulting from the lift. This will increase non-linearly with lift, or taper length, becoming constant when the lift reaches a steady value. It will include components from both the roof and bodyside taper and it is expected that each will follow, approximately, the same trend. The total drag, C_{DT}, will then vary with taper length, as shown, with drag initially reducing to a local minimum value followed by a drag rise to a local maximum when the lift reaches a steady value. The drag subsequently falls linearly as the base area reduces.

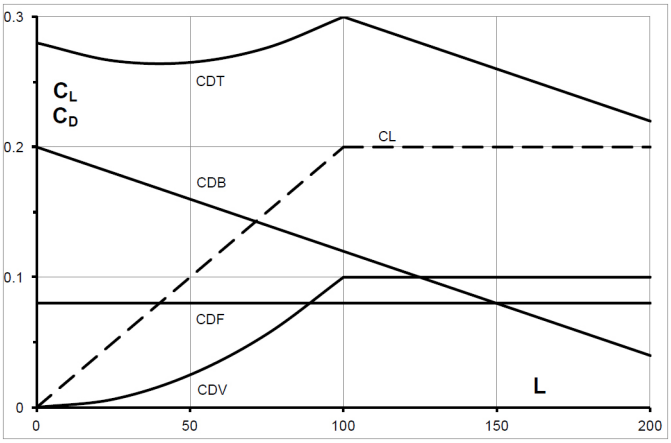

Figure 7. Proposed drag breakdown for a simple body with rear taper.

PIV was used to visualise the airflow immediately behind the body in the y-z plane. Results were obtained for only a few configurations and examples are shown in Figures 8(a) and 8(b) for two cases; the model with a 15° taper on the roof only and the model with a 15° taper on the roof and upper rear bodyside. The former case has a slope length of 222mm, which gives a taper length of 215mm, which is comparable to the latter case with a taper length of 225mm. Only time-averaged flow data is presented. Figure 8(a) shows the expected flow structure for a body with a sloping roof surface, with a strong vortex forming on the slant edge and downwash inboard of the edge vortex.

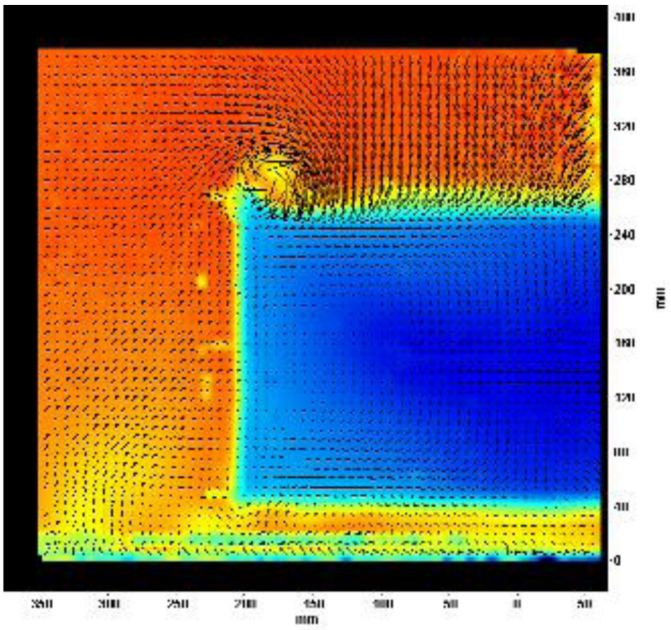

Figure 8(a). PIV in y-z plane at model trailing edge: 15° roof taper only.

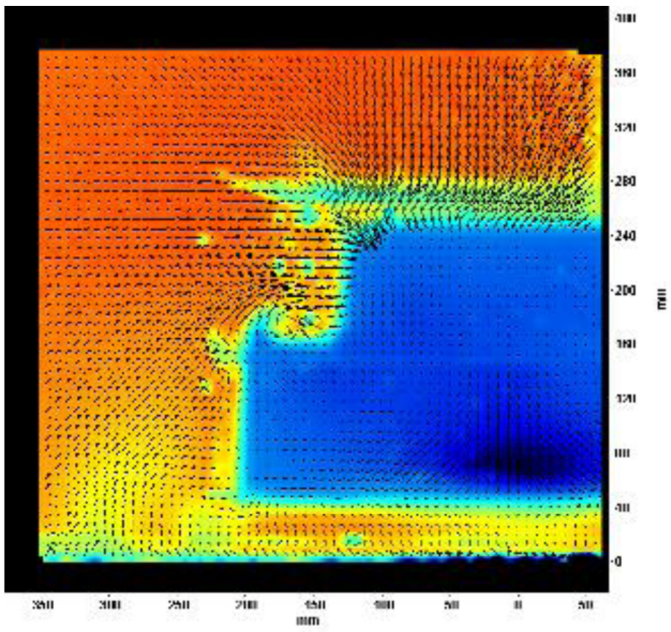

Figure 8(b). PIV in y-z plane at model trailing edge: 15° upper body taper

Figure 8(b) shows that with the addition of bodyside taper the roof edge vortex is largely suppressed, but a weak vortex is formed at the longitudinal junction of the tapered upper body and the untapered lower body. Downwash is present at the roof trailing edge, while an inflow occurs on the tapered bodyside. The inflow along the tapered side surface appears to draw air over the longitudinal edge on the top of the lower bodyside, generating a vortex of similar sign to that for the roof vortex in Figure 8(a), but of significantly reduced intensity.

Pressure measurements were also taken on the tapered surfaces and the base for a few configurations; the squareback model and the model with a 15° taper on the roof only, and the model with a 15° taper on the roof and upper rear bodyside for taper lengths of 125 and 225mm. The distribution of the pressure coefficients obtained on the rear body surfaces are shown in Figures 9(a) and 9(b), for the first two cases, respectively, and in Figures 10(a) and 10(b), for the tapered body cases with taper lengths of 125mm and 225mm respectively. The pressure coefficients are corrected for blockage. Only one half of the rear body is shown and the positions of the pressure tappings are identified by the black dots. The vertical dimension is taken from the ground plane.

The squareback model has significantly lower base pressure than the two tapered bodies. The rearward facing surfaces on the tapered bodies experience only suction loads, which generate drag. For the body with roof taper only, strong suctions are found along the roof slant leading edge, created by the flow acceleration as the slope changes and along the slant surface side edges, below the vortex shown in Figure 8(a).

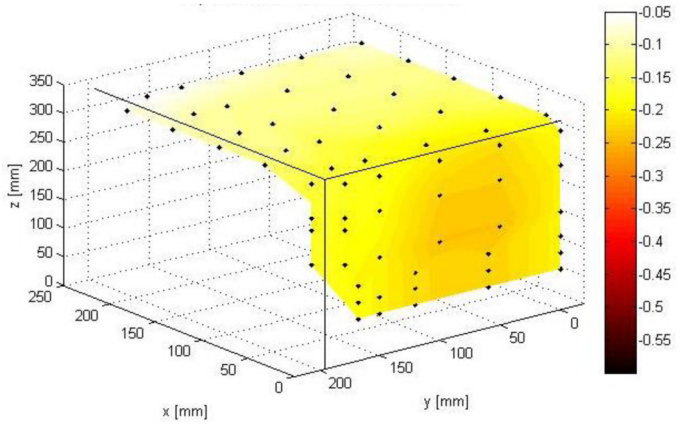

Figure 9(a). Surface pressure coefficients: Squareback model

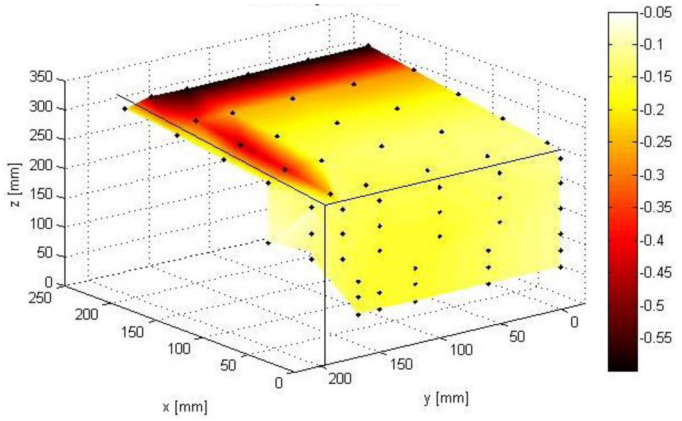

Figure 9(b). Surface pressure coefficients: 15° roof taper

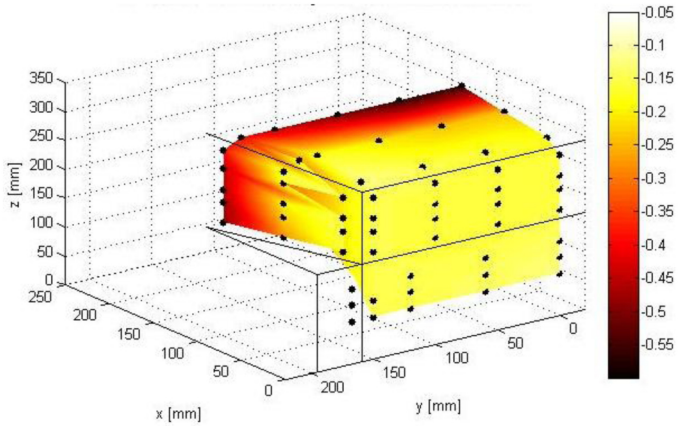

Figure 10(a). Surface pressure coefficients: 15° upper body taper, L=125mm.

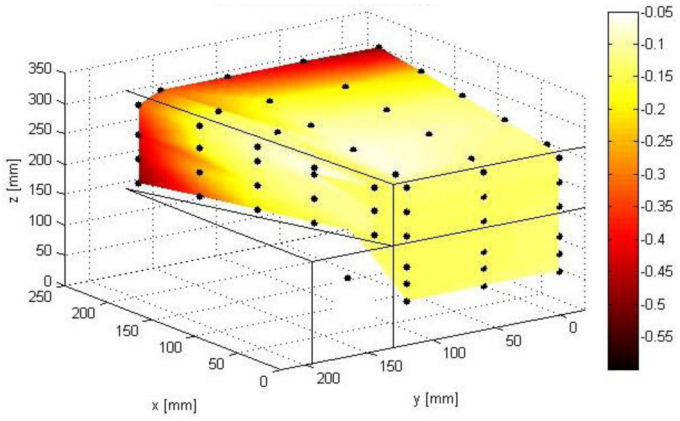

Figure 10(b). Surface pressure coefficients: 15° upper body taper, L=225mm.

For the two bodies with combined roof and bodyside taper the suction along the roof slant leading edge remains very similar to that shown for the body with roof slant only, but the suction on the roof side edges disappears, as the vortex is suppressed. A strong suction is also produced at the leading edge of the bodyside tapered section. The significant loading is similar for the two taper lengths, and with the loss of the lift created by the edge vortex, partly explains the constant lift experienced by taper lengths greater than 125mm. The drag component from these rearward facing tapered surfaces is concentrated at the leading edge of the taper and will grow only slightly as taper length increases.

Table 1. Mean Base Pressure Coefficients

Configuration	L	A_B	C_{PB}
Squareback	-	0.113	-0.206
15° Roof taper	215	0.090	-0.143
15° Roof and side taper	125	0.091	-0.150
15° Roof and side taper	225	0.077	-0.134

The average pressure coefficients, C_{PB}, obtained on the base for the four configurations, shown in Figures 9 and 10, are given in Table 1, where L is the taper length and A_B is the base area. The base pressure data presented are only approximate values for the mean base pressure coefficients, but they do show that tapering creates an increase in base pressure. It can also be noted that the base pressure coefficients for the two configurations with comparable base areas; one with side taper and one without, are very similar. This supports the suggestion from Howell and Le Good, [15], that base drag and, by inference, base pressure coefficients on tapered bodies are a function of the ratio of base area to frontal area. The significant change with increased taper length is the reduction in base drag resulting from the reduced base area and the increasing base pressure.

CONCLUSIONS

Wind tunnel tests have been conducted on a simple car-like shape, the Windsor body, to investigate the drag benefits from rear body taper. The tapered surfaces were confined to the upper rear body section and a range of taper angles and lengths were studied.

Drag and lift data are compared with the squareback model, which has no rear body tapering. For the range of taper angles and lengths investigated, drag reduces as taper angle is reduced and with taper length for longer lengths.

At shorter taper lengths an initial sharp reduction in drag occurs, but this trend is reversed and a local drag peak is experienced for taper angles greater than 10°. At large taper angles a significant increase in drag can occur for this taper length. A similar anomaly in the drag trend with taper length was identified for the body with roof taper only at one taper angle of 15°.

Lift increases with taper angle. For short taper lengths lift increases with length, but then becomes approximately constant as taper length increases further. The taper length at which the lift reaches a constant value coincides with the local peak in the drag trend.

Flow visualization with PIV shows that the longitudinal vortex formed on the rear pillars of the body with roof taper, but no side taper, is suppressed by the upper bodyside tapering, but a much weaker vortex is formed on the shoulder created by the side taper.

Pressure measurements indicate that a strong suction is formed at the intersection of the tapered rear surfaces and the flat roof and bodyside, which affects both drag and lift. Base pressure coefficients increase as base area is reduced and results in the reduction in base drag as taper length increases.

REFERENCES

1. Howell, J., Shape and Drag, Euromotor International Short Course; Using Aerodynamics to Improve the Properties of Cars. FKFS Stuttgart, February 17-18, 1998.
2. Pfadenhauer, M., Wickern, G., Zwicker, K., On the Influence of Wheels and Tyres on the Aerodynamic Drag of Vehicles. MIRA International Conference on Vehicle Aerodynamics, Birmingham, October 1996.
3. Viswanath, P.R., Flow Management Techniques for Base and Afterbody Drag Reduction. Prog. Aerospace Sci., Vol 32, pp79-129, 1996.
4. Howell, J., Sims-Williams, D., Sprot, A., Hamlin, F. et al., "Bluff Body Drag Reduction with Ventilated Base Cavities," *SAE Int. J. Passeng. Cars - Mech. Syst.* 5(1):152-160, 2012, doi:10.4271/2012-01-0171.
5. Morel, T., Effect of Base Cavities on the Aerodynamic Drag of an Axisymmetric Body. Aeronautical Qtly, 30, 400-412, 1979.
6. Englar, R., "Drag Reduction, Safety Enhancement, and Performance Improvement for Heavy Vehicles and SUVs Using Advanced Pneumatic Aerodynamic Technology," SAE Technical Paper 2003-01-3378, 2003, doi:10.4271/2003-01-3378.
7. Sykes, D.M., The Effect of Low Flow Rate Gas Ejection and Ground Proximity on After Body Pressure Distribution. Road Vehicle Aerodynamics, 1st Symposium The City University, London, November, 1969.
8. Howell, J., Sheppard, A., and Blakemore, A., "Aerodynamic Drag Reduction for a Simple Bluff Body Using Base Bleed," SAE Technical Paper 2003-01-0995, 2003, doi:10.4271/2003-01-0995.
9. Mair, W.A., Reduction of Base Drag by Boat Tailed Afterbodies in Low Speed Flow. Aeronautical Quarterly, Vol. 20, pp307-320, 1969.
10. Wong, D.T-M., Mair, W.A., Boat-tailed Afterbodies of Square Cross Section as Drag Reduction Devices. Journal of Wind Engineering and Industrial Aerodynamics, Vol. 12, pp229-235, 1983.
11. Gilhaus, A., Aerodynamics of Heavy Commercial Vehicles. Vehicle Aerodynamics Short Course 84-01, Von Karman Institute for Fluid Dynamics, Jan 1984.
12. Götz, H., Present and Future Trends in Automotive Aerodynamics. Vehicle Aerodynamics Short Course 84-01, Von Karman Institute for Fluid Dynamics, Jan 1984.
13. Cooper, K., "Truck Aerodynamics Reborn - Lessons from the Past," SAE Technical Paper 2003-01-3376, 2003, doi:10.4271/2003-01-3376.
14. Browand, F., Radovich, C., and Boivin, M., "Fuel Savings by Means of Flaps Attached to the Base of a Trailer: Field Test Results," SAE Technical Paper 2005-01-1016, 2005, doi:10.4271/2005-01-1016.
15. Howell, J. and Le Good, G., "The Effect of Backlight Aspect Ratio on Vortex and Base Drag for a Simple Car- Like Shape," SAE Technical Paper 2008-01-0737, 2008, doi:10.4271/2008-01-0737.
16. Johl, G., Passmore, M.A., Render, P.M., Design Methodology and Performance of an In-Draft Wind Tunnel. The Aeronautical Journal, Vol. 108, pp115-124, 2004.
17. Littlewood, R. and Passmore, M., "The Optimization of Roof Trailing Edge Geometry of a Simple Square-Back.," SAE Technical Paper 2010-01-0510, 2010, doi:10.4271/2010-01-0510.
18. Buchheim, R., Deutenbach, K., and Lückoff, H., "Necessity and Premises for Reducing the Aerodynamic Drag of Future Passenger Cars," SAE Technical Paper 810185, 1981, doi:10.4271/810185.
19. Han, T. Private communication, Dec 2012.

CONTACT INFORMATION

Jeff Howell
Senior Technical Specialist - Aerodynamics
Tata Motors European Technical Centre
International Automotive Research Centre
University of Warwick
Coventry CV4 7AL
UK
jeff.howell@tatamotors.com

ACKNOWLEDGMENTS

I thank Tata Motors European Technical Centre, TMETC, for permission to publish this paper. The initial research for the main part of this paper was funded by the Low Carbon Vehicle Technology Programme (LCVTP). The programme consisted of various workstreams and this project was part of Workstream 12, Aerodynamic Drag Reduction. I acknowledge the support of the workstream partners and TMETC as well as Geoff Le Good for establishing support from different universities. I thank Rob Hunter, Peter Stinchcombe, and Stacey Prentice from Loughborough University Department of Aeronautical and Automotive Engineering for making the model parts and supporting the wind tunnel tests. I also appreciate the contribution from Taeyoung Han, GM Research Labs, who provided an explanation of the drag trend highlighted in this paper.

DEFINITIONS/ABBREVIATIONS

A - Frontal Area

$\mathbf{A_B}$ - Base area

$\mathbf{C_D}$ - Drag coefficient

$\mathbf{C_{DB}}$ - Base drag coefficient

$\mathbf{C_{DF}}$ - Forebody drag coefficient

$\mathbf{C_{DT}}$ - Total drag coefficient

$\mathbf{C_{DV}}$ - Vortex drag coefficient

C_L - Lift coefficient

C_{MX} - Rolling moment coefficient

C_{MZ} - Yawing moment coefficient

C_P - Pressure coefficient

C_{PB} - Base pressure coefficient

C_Y - Side force coefficient

L - Taper length

Re - Reynolds number

z_0 - Ground clearance

φ - Taper angle